

Spray Away Allergies – Modeling Intranasal Drug Delivery

**BEE 4530
Computer Aided Engineering**

**By:
Michelle Chau
Pimkhuan Hannanta-Anan
Oleh Krupa
Jack Yi**

May 3rd, 2012

Table of Contents

1. EXECUTIVE SUMMARY	3
2. INTRODUCTION	4-5
2.1 DESIGN OBJECTIVES.....	5
3. PROBLEM FORMULATION	
3.1 TERMS DEFINED	5
3.2 SCHEMATIC	5-6
3.3 MESH.....	7
3.4 GOVERNING EQUATIONS	7-8
3.5 BOUNDARY CONDITIONS.....	8
3.6 ASSUMPTIONS	8
3.7 INPUT PARAMETERS	9-10
3.8 MASS TRANSPORT FORMULATION.....	10-11
4. RESULTS AND DISCUSSION	
4.1 RESULTS.....	11-13
4.2 LIMITATIONS TO RESULTS.....	13-14
4.3 ACCURACY TEST	14-15
4.4 SENSITIVITY ANALYSIS.....	15-17
5. CONCLUSIONS AND DESIGN RECOMMENDATIONS	
5.1 CONCLUSION.....	18
5.2 IMPLICATIONS AND RELEVANCE	18-19
5.3 DESIGN RECOMMENDATIONS	19
5.4 DESIGN CONSTRAINTS	19-20
6. APPENDIX A: MATEHMATICAL STATEMENT OF THE PROBLEM	
6.1 FORCE EXERTED ON PARTICLES FOR EVALUATION OF PARTICLE TRAJECTORIES	21
6.2 DERIVATION OF BOUNDARY CONDITION IN A NOSTRIL.....	21-22
7. APPENDIX B: SOLUTION STRATEGY	
7.1 MESH CONVERGENCE.....	23-24
8. APPENDIX C: SOFTWARE IMPLEMENTATION	
8.1 PARTICLE TRACING FUNCTION	25
8.2 PARTICLE COORDINATES	26
9. APPENDIX D: REFERENCES	27-28

1. Executive Summary

Nasal drug delivery has served as an alternative to oral and injection treatments for respiratory ailments, such as allergies, congestion, and infection (Berger, 2004). Recent studies have examined the role various parameters – spray particle size, flow rate in the nasal cavity, spray injection angle, injection velocity, material properties of the particle, and deposition mechanisms – play in alleviating nasal symptoms. It has been noted that certain specifications lead to wasteful drug deposition and ineffective delivery to targeted areas (Quraishi *et al.*, 1997). Computational models are vital in optimizing these parameters to maximize the drug's effectiveness in the targeted sinus areas. This study focuses on developing a computational model to describe the optimal flow rate, insertion angle, spray cone angle, and particle size of Azelastine hydrochloride (Astelin), a common anti-histamine drug, required to suppress an immune response while avoiding excessive drug application.

Assuming laminar airflow, the nasal cavity was modeled in 2D and divided into four regions: the anterior, the middle, the posterior, and escape. Using COMSOL Multiphysics 3.5a, the model implemented 2D Navier Stokes fluid flow equations and the Lagrangian Particle Tracing module to describe the distribution of drug in the nasal cavity. The particle deposition in the 4 regions depended on the characteristics of the particles and its flow. To validate the model output, the average drug concentration in each nasal cavity region was determined and compared with published numerical data analysis by Inthavong *et al.* (2008). We also run a mass transport simulation to observe the change in drug concentration in the mucosal layer over time.

Sensitivity analysis focused on average drug concentration to examine the effect of insertion angle, flow rate, cone spray angle, and particle diameter on drug deposition in the middle and posterior regions. Most drug particles are 50 μ m in size and it was determined that for this size, the combination of a 40 L/min flow rate of a high insertion angle of 45° and a large spray cone angle of 90° exhibited 100% optimal deposition in the posterior and middle regions. When particle size was decreased at higher flow rates, the majority of particles exited the outlet without depositing. For smaller sized particles, a lower flow rate of 20 L/min combined with a lower insertion angle of 20° and same spray cone angle of 90°, resulted in an optimal particle deposition of 64%.

These findings will allow future designs of nasal sprays to focus on the optimal parameters – drug size, flow rate, insertion angle, and spray cone angle. This model can pave a way for nasal sprays to be used in medical treatments outside of chronic rhinitis and respiratory ailments, such as diabetes and other pain treatments.

Keywords: *nasal spray, spray cone angle, drug deposition, Astelin, optimization*

2. Introduction

Nasal drug delivery provides an alternative non-invasive method to administer a variety of systemic drugs. The intranasal administration of drugs is not a novel concept, but has been practiced for centuries. Ancient Tibetans used inhalers containing sandalwood and aloewood extracts as antiemetic while Ancient Egyptians resorted to intranasal medicine to treat epistaxis and rhinitis (Quraishi *et al.*, 1997). This method of administration provides not only convenience to the patients, but also superior rates of drug absorption and metabolism in the mucosal lining of the nose.

The rich vasculature and high permeability of the nasal mucosa favor efficient pharmacokinetics, thus making it an ideal tissue to target for drug delivery. Factors that facilitate transnasal absorption of drugs include the stratified squamous epithelium of the nasal vestibule, the mucosa between nasal septum and lateral wall of the nose, and the vast absorption surface area provided by the pseudostratified columnar epithelium in the main vault of the nasal cavity (Quraishi *et al.*, 1997). In comparison to traditional intravenous or gastrointestinal administrations, pharmacologically active drug components are more stable in the nasal cavity environment, exhibit superior absorption in nasal mucosa, avoid hepatic elimination, circumvent the blood-brain barrier, and elude gastrointestinal and hepatic metabolism (Pires *et al.*, 2009). These advantages enhance drug bioavailability after absorption and allow sufficient medication to reach targeted regions.

Allergic rhinitis is a medical condition characterized by irritation and inflammation of the mucosal membrane in the nasal cavity. It's estimated that rhinitis affects 10%-30% of adults (Schoenwetter *et al.* 2004). Airborne allergens diffuse into the mucosal membrane where immune cells begin secreting antibodies as an allergic response. These antibodies bind to mast cells in the mucosal membrane, causing them to secrete histamine, which leads to itching, swelling, and mucus secretion in the nasal cavity. The most common treatment for rhinitis is by anti-histamines, which block histamine receptors on basophils and mucus-secreting mast cells to prevent inflammation. Nasal injection is the most effective method for drug delivery, as anti-histamines come into direct contact with the mucosal layer, without needing to diffuse through vasculature.

To maximize the advantages provided by nasal therapy, nasal drug delivery requires careful design of a nasal sprayer device. The ability of the sprayer device to deposit drug particles rely on fluid flow velocity, flow turbulence, deposition mechanisms between particles and environment, and particle properties stemming from particle density, size, and spray cone angle. The nasal sprayer must deliver administered drug to the posterior cavity for maximal absorption and avoid depositing in anterior regions where little drug diffuses through the mucosa. Recently, Inthavong *et al.* (2008) showed the major factors

influencing deposition – nasal cavity geometry, spray particle sizes, spray cone angles, insertion angle, and injected particle velocities – using a particle tracking method. The findings suggested that spray particle size, spray cone diameter, and insertion angle had significant effects on position of drug deposition.

Expanding on established studies, this report focuses on the optimal injection velocity/flow rate, injection angle, spray cone angle, and particle diameter. This model incorporates the Navier-Stokes and Continuity equations for fluid flow with Lagrangian Particle Tracking equations for particle velocity and location to observe concentration of drug deposited in the anterior, middle, and posterior cavity regions.

2.1 Design Objectives

We will model drug particle deposition in a simplified nasal geometry using mathematical modeling. We will determine the optimal injection flow rate, injection angle, spray cone angle, and particle mass and size for effective deposition of Azelastine hydrochloride in the posterior nasal cavity. The parameters are defined below in Problem Formulation. We will also observe how Azelastine is cleared from the mucosal layer. These findings will inform future nasal spray designs. Our goal is to identify what combination of parameters defined will lead to optimal drug deposition in the targeted nasal mucosa.

3. Problem Formulation

3.1 Terms Defined

Flow Rate – flow velocity of the particles as they enter the nasal cavity.

Particle Mass – the mass of the liquid particles injected by the nasal spray. Particle mass will depend only on particle diameter as the density is assumed to remain constant at 1000 kg/m^3 . Particle diameters range from $10\mu\text{m}$ to $50\mu\text{m}$.

Injection Angle – the angle at which the particles leave the spray nozzle and enter the nasal cavity

Cone Angle (Cone Diameter) – the angle from the nozzle at which particle spreading occur. In other words, it is the spray angle at which the liquid stream is dispersed into distinct particles. The cone diameter at which particle dispersion occurs is a function of cone angle.

3.2 Schematic

The anatomical image and geometry of the nasal passageway, shown in Figure 1, is simplified to a two dimensional geometry to reduce complexity in calculation. The simplified geometry consists of four distinct regions – the anterior, the middle, the posterior, and the escape. This model incorporates the appropriate parameters that determine whether spray particles will avoid being trapped in the anterior cavity and

reach the posterior areas instead. To account for computational discrepancies caused by sharper edges in a previous simplification, the design was adjusted accordingly using smooth boundary curves in Figure 2. This provided a more accurate representation of the true geometry and offered enhanced computational results.

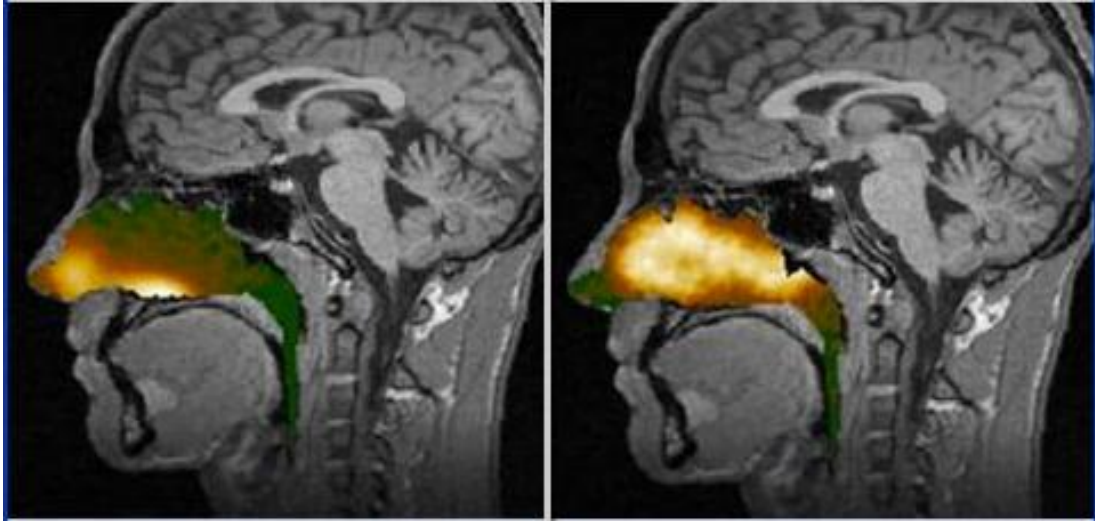


Figure 1. Anatomical image of a healthy human’s nasal cavity. The figure on the left shows current drug delivery in the nasal cavity in yellow. The figure on the right displays more efficient and improved drug deposition as seen by the nasal cavity being completely full. [http://www.optinose.no/nasal-delivery/nasal-delivery-challenges]

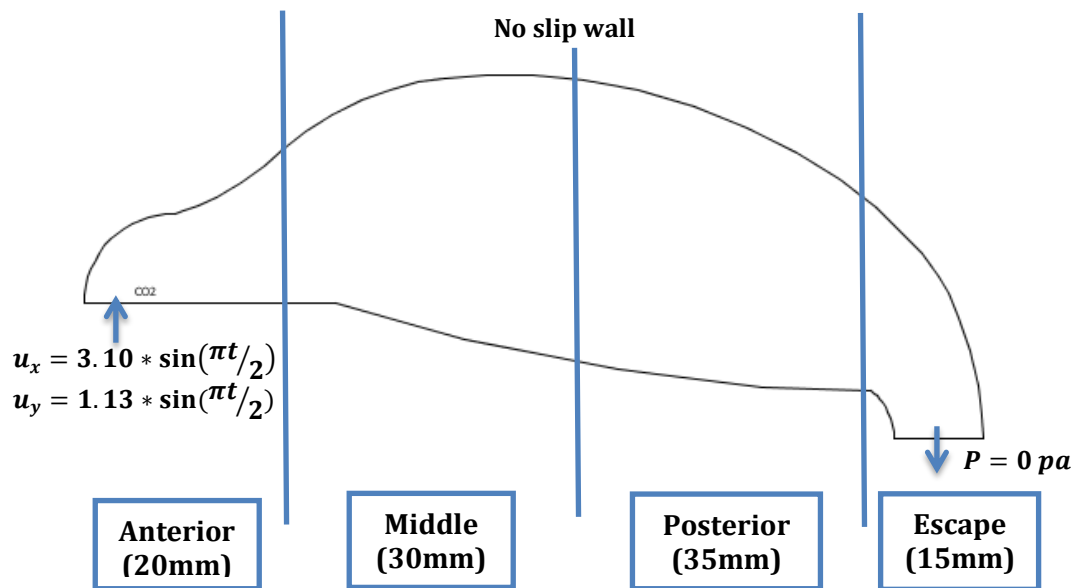


Figure 2. Simplified geometry of the nasal cavity and the flow boundary conditions. The cavity was divided into four regions based on distance along the x axis. The inlet velocity shown is one of the boundary conditions used in our model. The complete list of the nostril velocity can be found in table 3.

3.3 Mesh

Based on schematic from Figure 3, an unstructured mesh with an “extra fine” mesh size was applied to the geometry. A finer mesh was used around the edges to make sure particles were deposited in the proper regions along the boundary. The mesh contains a total of 5563 elements.

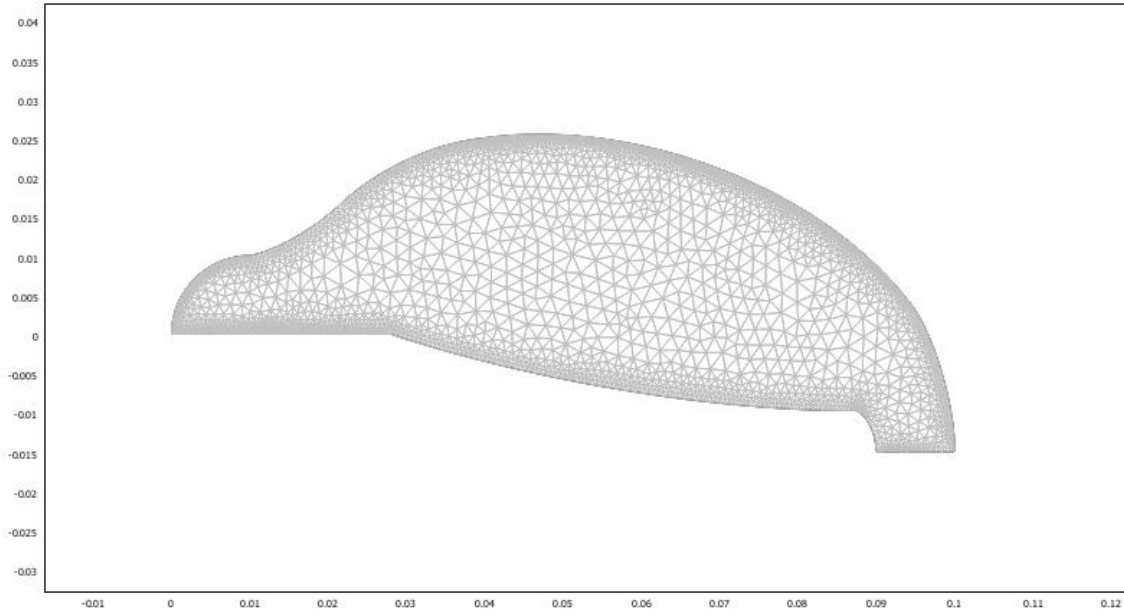


Figure 3. Unstructured mesh of nasal cavity model. Mesh contains 5563 elements.

3.4 Governing Equations

Fluid intake through the nose was modeled as a 2D laminar flow using the Navier-Stokes equation and the continuity equation for steady state conditions (Inthavong *et al.*, 2008). These equations are built into COMSOL as a module. The 2D species mass transport with the diffusive term and a zero order reaction was used.

Navier-Stokes and Continuity for Air Flow

$$\rho \frac{\partial u_x}{\partial t} + \rho \left(u_x \frac{\partial u_x}{\partial x} + u_y \frac{\partial u_x}{\partial y} \right) = -\frac{\partial p}{\partial x} + \mu \left(\frac{\partial^2 u_x}{\partial x^2} + \frac{\partial^2 u_x}{\partial y^2} \right) + \rho g_x$$

$$\rho \frac{\partial u_y}{\partial t} + \rho \left(u_x \frac{\partial u_y}{\partial x} + u_y \frac{\partial u_y}{\partial y} \right) = -\frac{\partial p}{\partial y} + \mu \left(\frac{\partial^2 u_y}{\partial x^2} + \frac{\partial^2 u_y}{\partial y^2} \right) + \rho g_y$$

$$\frac{\partial \rho}{\partial t} + \frac{\partial(\rho u)}{\partial x} + \frac{\partial(\rho v)}{\partial y} + \frac{\partial(\rho w)}{\partial z} = 0 \quad (\text{COMSOL Built-in equation})$$

Lagrangian Particle Tracing for Particle Velocity and Location

$$m_p \frac{du_p}{dt} = [F_d(u_g - u_p)]m_p$$

$$F_d = \frac{18\mu_g C_d Re_p}{24 \rho_p d_p^2}$$

$$Re_p = \rho_p d_p \frac{|u_p - u_g|}{\mu_g}$$

Species Mass Transfer

$$\frac{\partial c_a}{\partial t} = D_{AB} \left(\frac{\partial^2 c_a}{\partial x^2} + \frac{\partial^2 c_a}{\partial y^2} \right) + R_A$$

$$R_A = -(k_d + k_c)c_0$$

3.5 Boundary Conditions

Flow Boundary Conditions

- Nasal wall is rigid
- Effect of mucus is negligible
- No-slip condition at the cavity wall
 - Velocity of fluid at cavity wall is zero
- Average inspiratory flow rate varying from 20 to 40 L/min
- Pressure at outlet is assumed to be 0 Pa

Diffusion Boundary Conditions

- Mucus layer completely insulated from nasal cavity and epithelium

3.6 Assumptions

Flow assumptions were adapted from Inthavong *et al.* (2008).

Fluid Flow

1. Laminar flow
2. Air flow in nasal cavity is modeled as Newtonian and incompressible fluid.

Particles

1. All particles are assumed to be spheres of the same size
2. Particles are trapped with 100% efficiency once in contact with the cavity wall
3. Negligible gravitational forces on particles

Mass Transport

1. Drug does not evaporate from mucosal layer into the nasal cavity
2. Drug elimination modeled as zero order elimination reaction
3. Convective flow ignored at the boundary and out of the mucus layer is ignored
4. Mucosal layer thickness is constant throughout the boundary
5. Drug concentration is initially constant across the width of the mucosal layer.

3.7 Input Parameters

The input parameters and units used are shown in Table 1, 2, 3, and 4. Table 1 consists of constant values.

Table 1. Constant Input Parameters

Particle Density	ρ_p	1000 kg/m ³	(Inthavong <i>et al.</i> , 2008)
Initial Particle Velocity	$u_{p,x}$	0 m/s	(Inthavong <i>et al.</i> , 2008)
	$u_{p,y}$	0 m/s	(Inthavong <i>et al.</i> , 2008)
Initial Fluid Velocity	$u_{g,x}$	0 m/s	(Inthavong <i>et al.</i> , 2008)
	$u_{g,y}$	0 m/s	(Inthavong <i>et al.</i> , 2008)
Drag Force Coefficient	C_d	0.44	(Holland <i>et al.</i> , 1995)
Fluid Viscosity at 290K	μ_g	1.7985 x 10 ⁻⁵ kg/m·s	(Datta and Rakesh <i>et al.</i> , 2008)
Fluid Density at 290 K	ρ_g	1.2177 kg/m ³	(Datta and Rakesh <i>et al.</i> , 2008)
Drug Diffusivity in mucosal layer	D	1.5 x 10 ⁻¹⁰ m ² /s	(Desai <i>et al.</i> , 1991)
Partition Coefficient	K	293.7	https://www.ebi.ac.uk/chembl/db/index.php/compound/inspect/CHEMBL639
Drug Degradation Rate	k_d	6.0312*10 ⁻⁶ s ⁻¹	https://www.ebi.ac.uk/chembl/db/index.php/compound/inspect/CHEMBL639
Total Drug Injected During One Spray	c_0	3.59 x 10 ⁻⁴ mmol	https://www.ebi.ac.uk/chembl/db/index.php/compound/inspect/CHEMBL639

Table 2 consists of different input parameters that were used in the sensitivity analysis.

Table 2. Varying Constant Input Parameters (Inthavong *et al.*, 2008)

Particle Diameter	d_p	5, 10, 20, 50 μ m
Spray Cone Diameter	d_{in}	2, 4, 6, 10 mm
Flow Rates	Q	20, 30, 40 L/min
Average Velocity	u_{avg}	2.1, 3.15, 4.2 m/s

Table 3 consists of equations representing velocity as a function of time with different insertion angles. These time-dependent inlet velocities were set as boundary conditions at the nostril. We used a sine function to model the breathing pattern more accurately.

Table 3. Velocity as a Function of Time Relative to Insertion Angles

Insertion Angle (°)	Flow Rate (L/min)			
		20 ($u_{avg}=2.1$ m/s)	30 ($u_{avg}=3.15$ m/s)	40 ($u_{avg}=4.2$ m/s)
20	u_x	$3.10 * \sin(\pi t/2)$	$4.72 * \sin(\pi t/2)$	$6.20 * \sin(\pi t/2)$
	u_y	$1.13 * \sin(\pi t/2)$	$1.72 * \sin(\pi t/2)$	$2.26 * \sin(\pi t/2)$
30	u_x	$2.86 * \sin(\pi t/2)$	$4.36 * \sin(\pi t/2)$	$5.72 * \sin(\pi t/2)$
	u_y	$1.65 * \sin(\pi t/2)$	$2.52 * \sin(\pi t/2)$	$3.30 * \sin(\pi t/2)$
45	u_x	$2.33 * \sin(\pi t/2)$	$3.56 * \sin(\pi t/2)$	$4.67 * \sin(\pi t/2)$
	u_y	$2.33 * \sin(\pi t/2)$	$3.56 * \sin(\pi t/2)$	$4.67 * \sin(\pi t/2)$

Table 4 consists of mucosal clearance rates that were used to model drug elimination from the mucus layer. Rates were considered constant based on *in vivo* experimental data from Hua (2010). Note that these rates are based from a mouse model with elimination of nanoparticles in isotonic saline.

Table 4. Mucosal Clearance Properties

Time	Mucosal Clearance Rate (k_c)	
0 to 10 min	$1.7\% \text{ min}^{-1}$	(Hua <i>et al.</i> , 2010)
10 to 60 min	$0.3\% \text{ min}^{-1}$	(Hua <i>et al.</i> , 2010)

3.8 Mass Transport Formulation

After performing the flow simulation, species mass transport calculations were done in the mucosal layer. The mucosal layer was estimated to be 0.5mm in thickness (Marttin *et al.* 1998). The particle distribution along boundary was calculated by interpolating particle deposition along the boundary. Particle coordinates were determined (see Appendix 8.2) and were the basis for the areas of 25 subdomains in mucosal layer where particles had deposited (Figure 4, Table 5). Each particle coordinate was positioned at the midpoint of the width of each subdomain. By dividing the total drug injected by the mucus area, the total drug concentration was determined to be 4.03 mmol/m^2 . Each subdomain contained a fraction of the initial concentration, based on the area of the subdomain.

Drug removal was assumed to occur by two modes: elimination from mucus turnover and drug degradation. Hua *et al.* observed that mucosal clearance occurs at 2 relatively constant rates within the first hour. Therefore, we used a zero order reaction to model drug elimination from the mucosal layer. This reaction incorporated the elimination rate and the initial concentration in each subdomain.

Table 5 consists of mucosal subdomain areas and initial concentration determined by particle distribution along the boundary. Note that the particle distribution in this model was based on the flow model with optimal deposition parameters (40L/min, 45° insertion, 6 mm cone, $50 \mu\text{m}$ particle diameter), where all particles had deposited in the cavity.

Table 5. Mucosal Subdomain Initial Concentrations Along The Upper Boundary

	1	2	3	4	5	6	7	8	9	10	11	12	13
Area (10^6 m^2)	5.06	2.1	1.58	1.33	1.26	0.921	0.834	0.736	0.622	0.618	0.573	0.537	0.535
Concentration (10 mmol/m^2)	0.028	0.068	0.090	1.08	1.13	1.56	1.71	1.94	2.29	2.31	2.49	2.66	2.66
	14	15	16	17	18	19	20	21	22	23	24	25	Total
Area (10^6 m^2)	0.505	0.536	0.533	0.530	0.537	0.556	0.553	0.556	0.572	0.618	0.610	4.02	26.8
Concentration (10 mmol/m^2)	2.82	2.66	2.66	2.73	2.65	2.56	2.57	2.56	2.48	2.29	2.32	0.354	50.4

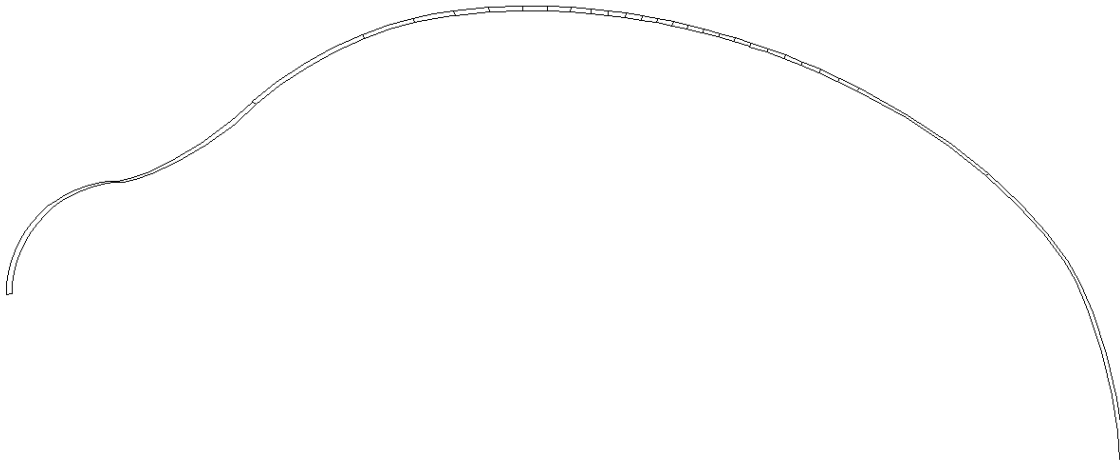


Figure 4. Schematic of mucosal layer divided into multiple subdomains. Note that only the top boundary was considered as no particles deposited along the bottom boundary.

4. Results and Discussion

4.1 Results

We ran our model for a range of flow rates from 20 L/min to 40 L/min, insertion angles from 20° to 45°, spray cone diameters from 2mm to 8mm, and varying particle diameters from 10 μ m to 50 μ m. Comparing combinations of these parameters, an optimal combination for maximum drug deposition was achieved at 40 L/min flow rate with a 45° insertion angle and a 90° (6mm) cone angle. Figure 5 shows the contour plot for fluid flow through nasal cavity based on said parameters.

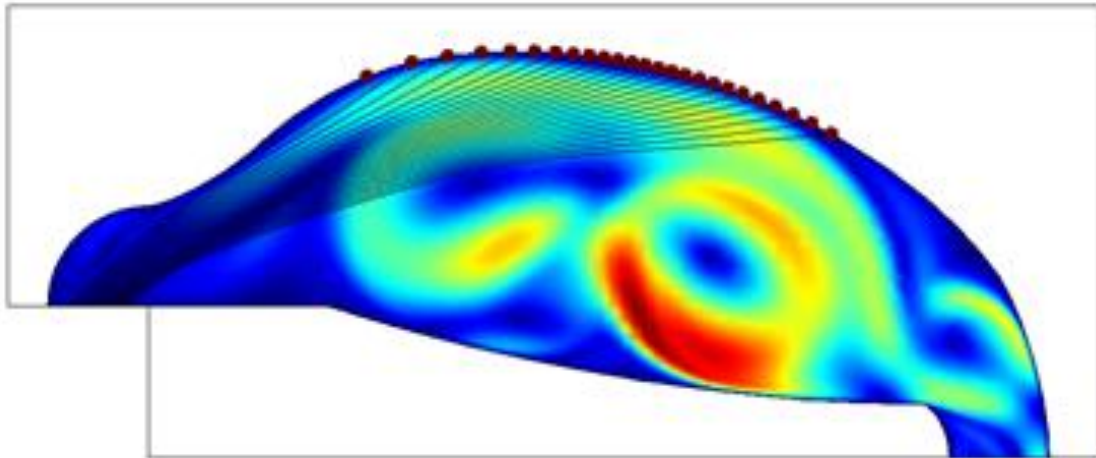


Figure 5. Contour map of nasal cavity with fluid flow, drug deposition, and particle tracking. The optimal parameters of 40 L/min flow rate, with a 45° insertion angle and a 90° cone angle (6mm) were used.

Furthermore, the model was expanded to test diffusion and elimination of the drug after deposition into the surrounding mucosal layer. Figure 6 shows the concentration profile after 1 hour based on the particle distribution profile from the flow simulation with optimal parameters. The average drug concentration distribution in each subdomain is given in Figure 7.

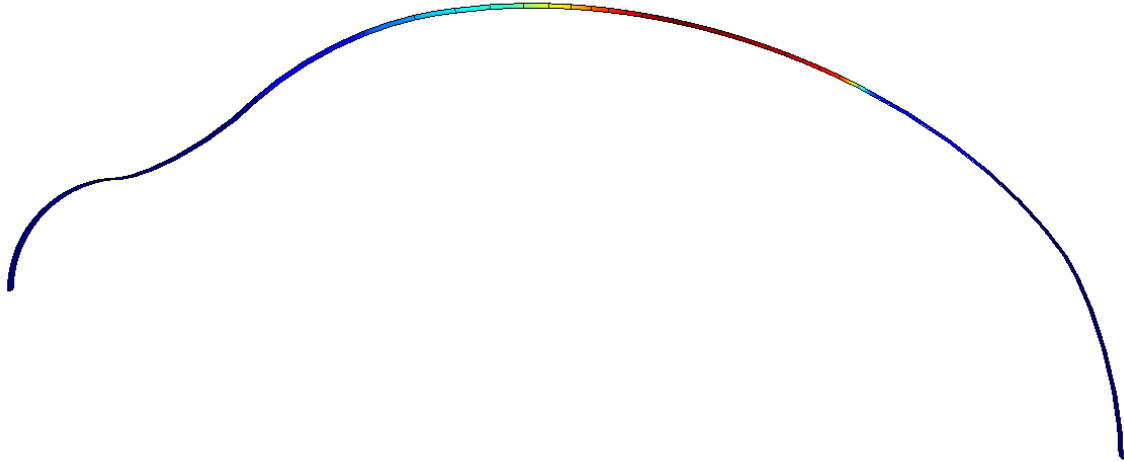


Figure 6. Contour map of drug concentration after 1 hour. This simulation was based on the drug deposition from the optimal case shown in Figure 4.

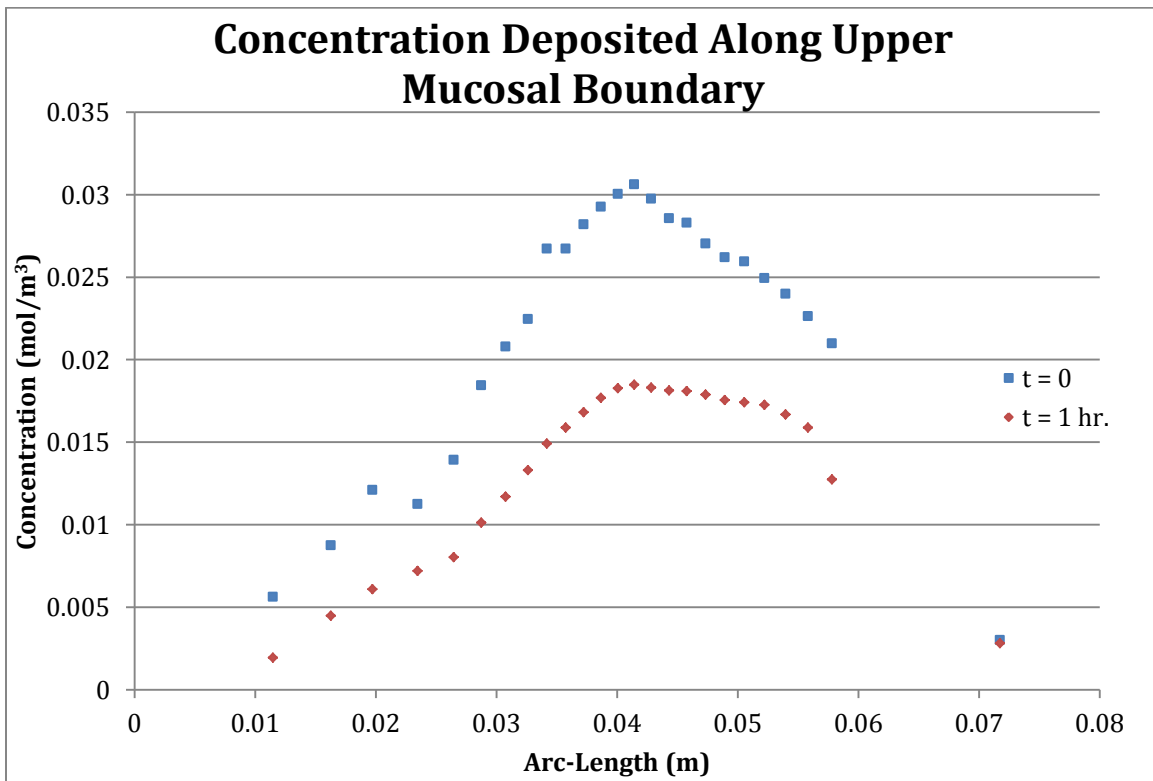


Figure 7. Plot of average drug concentration in each subdomain at $t=0$ and $t=1$ hr. Note that subdomains were only evaluated where drug was deposited at the upper boundary, not the entire mucosal layer. Over time, drug is eliminated and diffuses out resulting in a flatter profile.

The contour map and concentration profile suggest that diffusion will have a role in spreading drug throughout mucosal layer. However, the rate of elimination is much too fast for the drug concentration to have a completely even spread throughout the layer. From the total average concentration plot (Figure 8), one can see that the drug is eliminated quickly in the first 10 minutes and more slowly after 10 minutes. Our model predicts that 32.3% of the drug is eliminated after 1 hour.

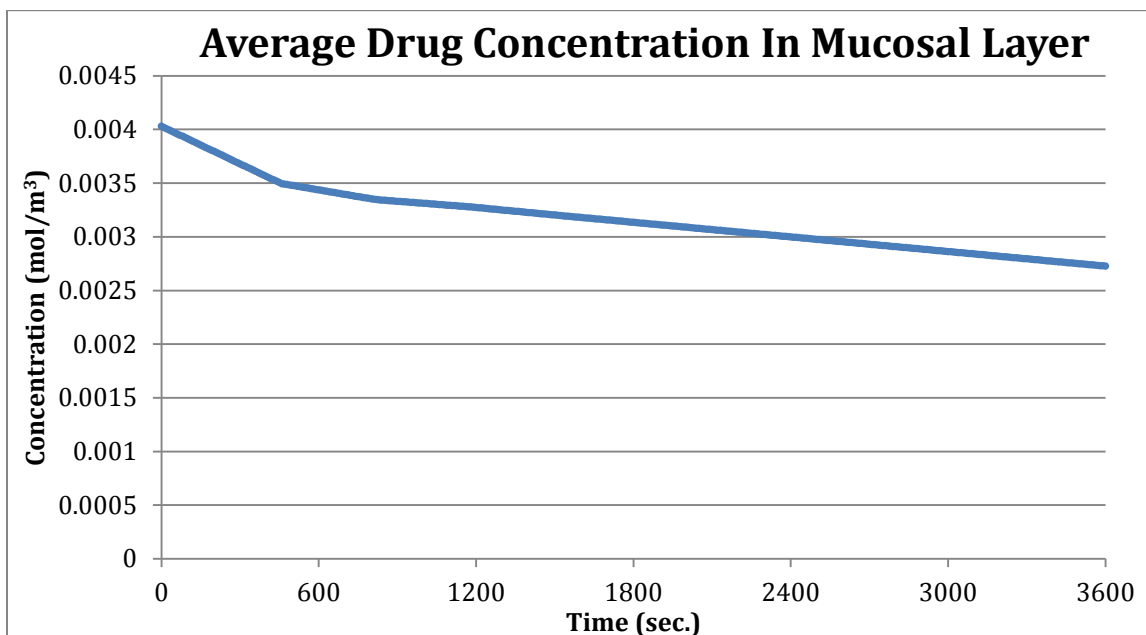


Figure 8. Plot of average drug concentration in the entire mucosal layer over time (including the areas for the top and bottom layers of nasal cavity). The fastest rate of elimination occurs in the first 10 minutes.

4.2 Limitation of Results

There were several limitations to our results. The model was limited to one cycle of breathing because COMSOL would have had difficulty converging and solving the problem. The initial fluid velocity was assumed to be 0 m/s because if the initial velocity was significantly higher it would be more likely for the drug particles to deposit in the anterior region instead of the middle and posterior region. This initial fluid velocity value was also not realistic. We are constantly breathing in and out so it would be impossible for the velocity at the inlet of the nasal cavity to ever be 0 m/s.

Another limitation was in our diffusion analysis. The drug concentration profile was determined by interpolating particle deposition, instead of using a more accurate, continuous distribution. Increasing the number of particles would provide more accurate results, but becomes more time intensive. Also, flow effects were not considered and elimination was considered as a zero order reaction, while in reality elimination also must

depend on drug concentration. Yet another limitation was assuming drug concentration was homogeneous in each subdomain.

4.3 Accuracy Check

To confirm the accuracy of our flow results, we compared with a similar computational model (Inthavong *et al.*, 2008) and an experimental model (Cheng *et al.*, 2001). Specifically, we looked at particle deposition along different sections of the nasal boundary. Using the postprocessing particle tracing module, 50 particles at 10 μ m diameter were released for 2 seconds. The nasal cavity, depicted in Figure 9, was divided into 4 sections: anterior, middle, posterior, and escape. Our model assumed perfect particle entrapment along the boundary.

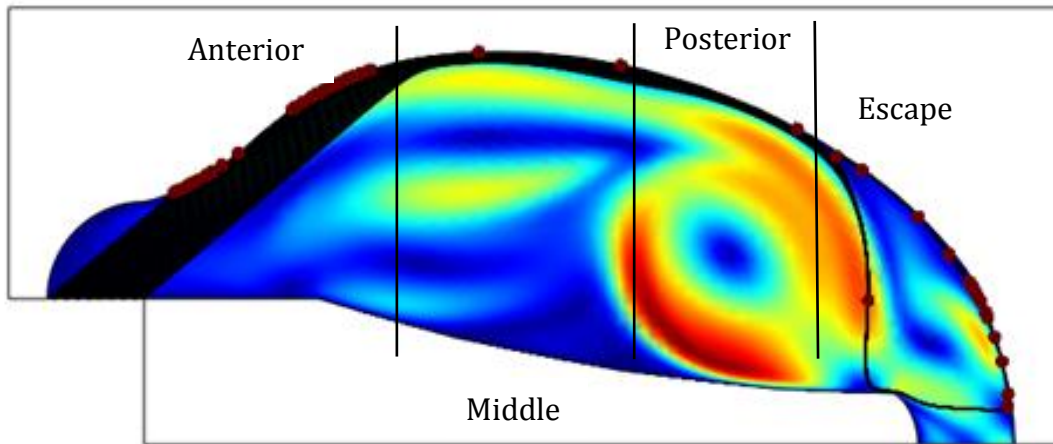


Figure 9. Accuracy check of nasal cavity model. The number of drug particles stuck to the wall of the nasal cavity in each of the four regions – anterior, middle, posterior, and escape – are shown. Parameters used were equivalent to those used by Inthavong.

Table 6. Percentage of Drug Particles Captured in Each Nasal Region

	Anterior	Middle	Posterior	Escape
Number of Particles	30	2	4	14
Fractional Deposition	0.6	0.04	0.08	0.28
Ithavong, 2008	0.538	0.036	0.038	0.388
Error	+11.5%	+11.1%	+111%	-27.8%
Chen, 2003	0.375	0.625	0	0

Our results shown in Table 6 have a similar trend as seen by Ithavong *et al.*, (2008). Most of the particles either deposited in the anterior region or escaped through the outlet. The relatively high error values can be accounted for by the small differences in geometry. Better accuracy can be achieved with more particles, but visualization and particle tracking would be significantly more difficult.

On the contrary, our results were significantly different from to Cheng *et al.*, (2003). The middle portion, in Cheng's findings, had absorbed more particles. A number of factors that could have contributed to variation from experimental data include particle diameters, a 3D geometry, a lower inlet flow rate, and turbulence. Our particle deposition was very sensitive to particle diameter as seen in our sensitivity analysis. The 3D geometry would increase the surface area and consequently cause most of the particles to become entrapped before leaving the nasal cavity.

Unfortunately, we could not find any other studies that analyzed elimination of anti-histamines in the mucosal layer. Measuring total drug concentration in the nasal cavity over time is still very difficult to achieve *in vivo*. However, our cumulative drug clearance (32.3%) did compare favorably with those observed by Hua *et al.* 2010 (33.2%), who performed mucosal clearance tests of isoflurane at an equal concentration in the mouse model.

4.4 Sensitivity Analysis

Our sensitivity analysis analyzed the effects of four parameters on drug deposition: flow rate, insertion angle, cone diameter, and particle diameter. Our analysis determined the optimal parameters for deposition in the middle and posterior regions of the nose. Parameter values were adapted from Inthavong *et al.*, (2008). The model implemented at three inlet flow rates (20, 30, 40 L/min), which were converted to flow velocity as shown in Appendix A. Insertion angle was varied by changing the x and y components of the flow velocity at the inlet. Parameters in the particle-tracing module were varied to account for different cone and particle diameter. Combinations of four different insertion angles and cone diameters were tested (Figure 10).

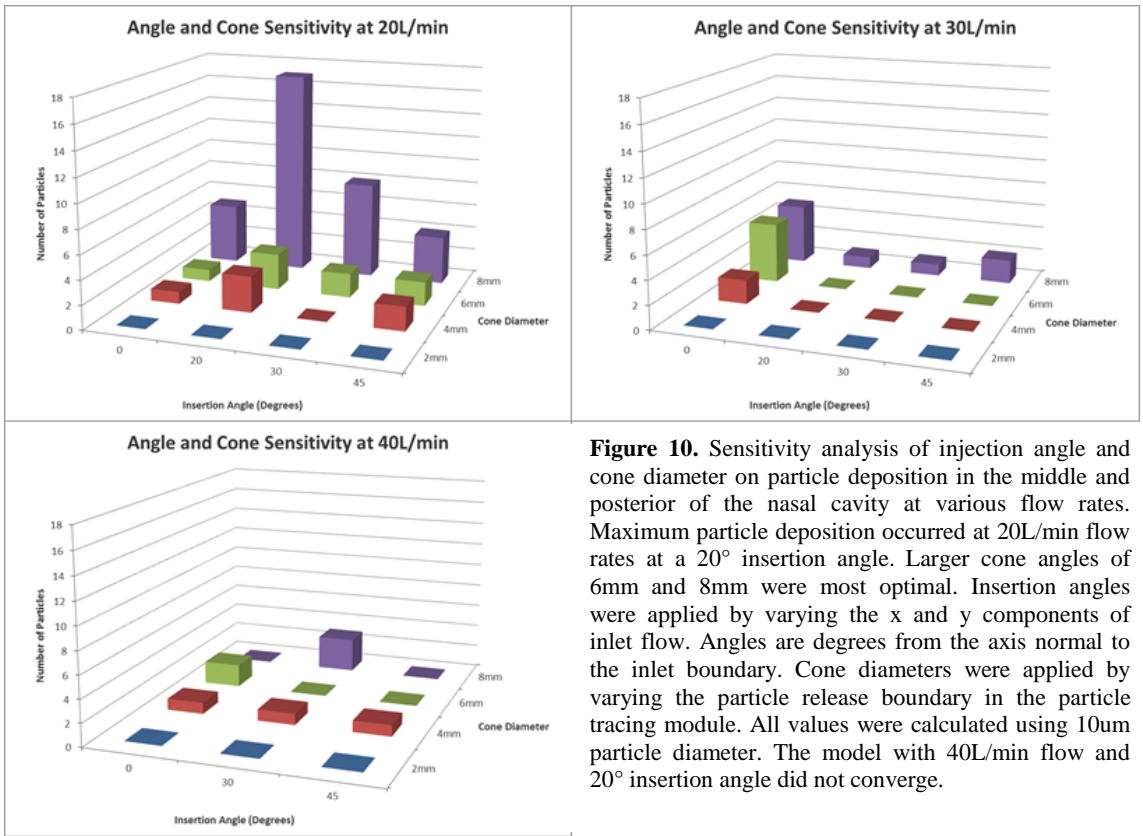


Figure 10. Sensitivity analysis of injection angle and cone diameter on particle deposition in the middle and posterior of the nasal cavity at various flow rates. Maximum particle deposition occurred at 20L/min flow rates at a 20° insertion angle. Larger cone angles of 6mm and 8mm were most optimal. Insertion angles were applied by varying the x and y components of inlet flow. Angles are degrees from the axis normal to the inlet boundary. Cone diameters were applied by varying the particle release boundary in the particle tracing module. All values were calculated using 10um particle diameter. The model with 40L/min flow and 20° insertion angle did not converge.

Our results showed the most deposition occurring at 20L/min with a 20° insertion angle. Deposition also seemed to occur more frequently at higher cone diameters. Particle diameter directly increased the particle mass when the density remained constant. Next, the optimal combination for each flow rate was tested with varying particle diameter sizes. Our results are shown in Figure 11.

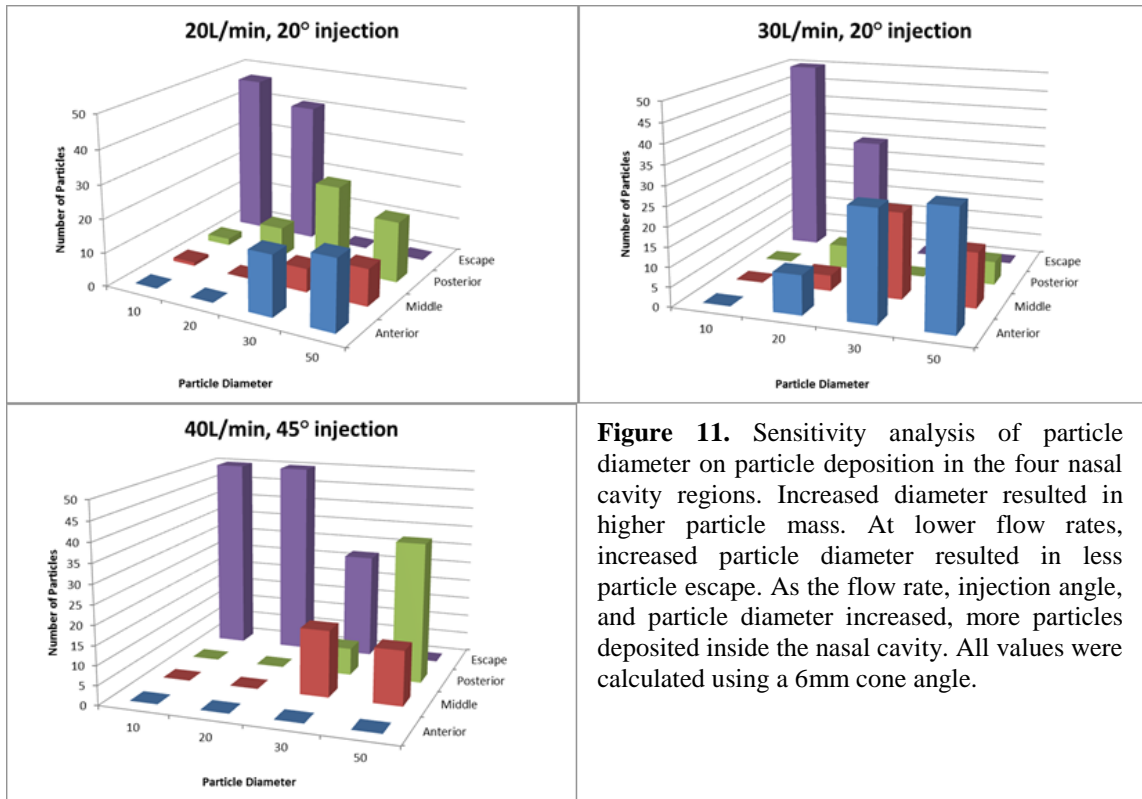


Figure 11. Sensitivity analysis of particle diameter on particle deposition in the four nasal cavity regions. Increased diameter resulted in higher particle mass. At lower flow rates, increased particle diameter resulted in less particle escape. As the flow rate, injection angle, and particle diameter increased, more particles deposited inside the nasal cavity. All values were calculated using a 6mm cone angle.

At lower flow rates, increased diameter increases particle deposition in the nasal cavity only by a little. This occurred because the high particle mass caused particle to move less directly along the flow and prevent escape through the outlet, but the particle was too heavy for the low flow rate to bring the drug to the target location. At lower masses, there was more circulation as particles escaped along Eddy currents occurring along the sides of the main flow path. At high flow rates, deposition increased with particle diameter as increased velocity allowed particles to have more momentum to escape the flow path and deposit along the top boundary. By varying the angle, one can “aim” the particle deposition path. Our model shows that maximum particle deposition at the middle and posterior regions occur when “aiming” the flow at a 45° insertion angle.

5. Conclusion and Design Recommendations

5.1 Conclusion

This study demonstrated the significance of insertion angle in determining deposition of spray particles in the middle and posterior regions of the nasal cavity. For a flow rate of 20 L/min, maximal deposition occurred with an insertion angle of 20°. However, when we varied flow rate from 20 L/min to 30 L/min to 40 L/min, maximum particle deposition occurred at insertion angle of 45°. As the particle diameter increased, the mass of the drug increased as well. This change required a higher flow rate and larger insertion angle for the drug to be deposited effectively in the middle and posterior regions. Also, our mass transport simulation showed that drug elimination occurs much too rapidly before the drug concentration can evenly spread by diffusion.

5.2 Implications and Relevance

Our model demonstrated the importance of the size of drug particles, which ultimately decides the flow rate and insertion angle most suitable for administration. While the typical drug particle diameter should never be as large as 50µm but not too small, a size of 10 or 20µm is also reasonable. This consequently dictates a lower flow rate and a smaller insertion angle to prevent too many particles from escaping through the outlet.

This finding helps considerations for drug dosages when evaluating the reproducibility and precision of the delivery of the spray. In the case of Azelastine hydrochloride, the recommended dosage for adults and children 12 years of age and older is one or two sprays per nostril twice daily (Berger, 2009). Each spray, delivering 137 µg of drug, significantly reduces histamine release and biochemical regulators of inflammatory response. Thus, our parameters can dictate an effective combination that will deliver the prescribed amount to targeted areas.

In addition, the cone angle and insertion angle parameters are useful in developing head positioning techniques for administering Azelastine hydrochloride. The current positions are: 1) head neutral (0-10° to the vertical plane), spray at 30° to the plane of face and 2) head forward (60-90° to the vertical plane), spray at 90° to the plane of face (Bateman *et al.* 2002). Bateman pointed out that neither technique is superior to the other and both fail to deliver optimal distribution of drug to posterior nasal cavity. Our findings can improve clinical studies and provide proper insertion and cone angles for maximal delivery of drug to the posterior regions.

Most importantly, this study paves a way for nasal sprays to be used in medical treatments outside of chronic rhinitis and respiratory ailments. In past and recent scientific news nasal sprays have been involved in a range of treatments. They have been

used to incorporate the use of vasopressin to treat diabetes insipidus. Results have shown that the method of treatment allows the drug to stay in blood plasma longer and its absorption is effective, non-sensitive, and non-irritating. It could be used as an in between treatment for patients with severe diabetes (Dashe, 1964). Also nasal decongestants can be used to significantly reduce the frequency of snoring (Braver *et al.*, 1995). Most recently, research has begun for the use of intranasal fentanyl for treating acute pain. The benefit of this administration is an immediate effect on the central nervous system and it can be administered to children as well. However, the onset time so far is longer than the basic IV treatment. More studies have to be done to incorporate pharmacokinetics to allow faster and more efficient absorption. Some other hypotheses being worked on now involve a nicotine replacement treatment by nasal spray instead of a patch or pill, and a nose to brain drug delivery pathway to avoid the blood brain barrier. Our results on optimal parameters for maximum absorption will help with the amount of research going into nasal sprays utilizing different drugs to treat various types of illnesses and the pharmacokinetics that come along with the types of drugs used, which need to be studied and taken into account.

5.3 Design Recommendations

Based on our study we determined that effective drug deposition for a moderately sized around 10 to 20 μm drug particle requires a flow rate of approximately 20 L/min and an insertion angle of 20° . For most drug particles sized at 50 μm , a flow rate of 40 L/min and insertion angle of 45° showed higher effectiveness. The spray cone diameter should always be at least 6 mm, which is a 90° spray angle. We would recommend designers of nasal sprays to make the nozzle longer and possibly narrower. The longer length would help achieve the small insertion angle. On the other hand, the outlet of the nozzle for the drug particles should be designed for the particles to produce the optimal spray cone diameter. Also, nasal spray development should not put too much focus on improving diffusion because this rate is several orders of magnitude slower than the mucosal clearance rate.

5.4 Design Constraints

Although our model found the optimal spray and drug parameters of Azelastine, the values used may not apply to other drugs. Different drug applications have different particle densities, drug diffusion coefficients, and particle sizes. The variability in particle densities would affect the modeling of drug deposition. If the drug is lighter, a lower inlet velocity is required with a lower insertion angle. But if the drug is heavier, a higher flow rate along with a higher insertion angle can be used to achieve the same percentage of drug deposition in the middle and posterior regions. Also the difference in diffusion coefficients may be representative of the mechanisms of different drugs. However, it is difficult to obtain the values of these diffusion coefficients from experimentation. Another factor to consider is the mucosal layer. This layer constantly changes its

chemical composition and thickness, affecting viscosity, drug distribution, and therefore diffusion rates. Some current intranasal applications do not deposit particles at a fairly constant particle size. This high degree of variability brings up questions on how accurate any computational model can be in determining a definite set of optimal parameters.

Another constraint to our model was using 2D geometry instead 3D. With modern day technology, it is easier to scan a patient's nasal cavity to serve as a 3D model. However, the governing equations and input parameters used for flow velocity would be more complex. This would change the equations in our model and the solution time would be much longer. On the other hand, a 3D model would provide observations and results that would be much more accurate than our 2D geometry. Significant effort should be put into developing a 3D model as it's clear from anatomical imaging that the 3D model would have a much greater surface than a 2D model projected as a slab. Surface area is arguably the most important difference will significantly affect where particles get deposited. While it may be challenging to develop a functional 3D model, this is the clear next step in modeling intranasal delivery

6. Appendix A: Mathematical Statement of Problem

6.1 Force exerted on particles for evaluation of particle trajectories

$$F = m_p \frac{du_p}{dt} = [F_d(u_g - u_p)]m_p$$

$$F_d = \frac{18\mu_g C_d Re_p}{24 \rho_p d_p^2} = \frac{18\mu_g C_d \left(\rho_p d_p \frac{|u_p - u_g|}{\mu_g} \right)}{24 \rho_p d_p^2} = \frac{3C_d |u_p - u_g|}{4 d_p}$$

Plug in the F_d equation into the force equation, we get

$$F = \left[\left(\frac{3C_d |u_p - u_g|}{4 d_p} \right) * (u_g - u_p) \right] m_p$$

This derived force equation was inputted into the equation of motion of the particle tracing function in COMSOL to obtain the pattern of drug deposition (see figure 9.)

6.2 Derivation of boundary condition at a nostril

Flow rate in human nasal passageway ranges between 20 and 40 L/min which correspond to average inlet velocity of 2.1 m/s and 4.2 m/s (Inthavong *et al.*, 2006). Because the physiological flow velocity is not constant over a breathing cycle, we sought to apply a time-dependent velocity to the boundary condition at the inlet, while keeping the average velocity at the physiological rates.

To derive the inlet velocity equation, we first looked at the general form of sine equation.

$$u = \text{amplitude} * \sin(2\pi t/T)$$

where u is velocity

t is time

T is a period of one breathing cycle (which is 4 seconds for human)

We next calculated the function of average velocity

$$U_{\text{avg}} = \frac{\int_0^{t_f} u dt}{t_f} = \frac{\int_0^{t_f} A * \sin(2\pi t/4) dt}{t_f}$$

$$= \frac{-\frac{2A}{\pi} \cos\left(\frac{\pi t}{2}\right)}{t_f} \Bigg|_0 \text{ to } t_f = 2 \text{ s}$$

Note that we modeled only half of the breathing cycle. Our final time is therefore equal to 2 seconds

$$u_{avg} = 2A/\pi$$

We knew the value of average velocity and we wanted to find amplitude value. Rearranging the equation, we got:

$$A = u_{avg} * \pi / 2$$

Plugging the equation of amplitude back into the original speed equation, we got:

$$u = \frac{u_{avg}\pi}{2} \sin(\pi t/2)$$

7. Appendix B: Solution Strategy

7.1 Mesh Convergence

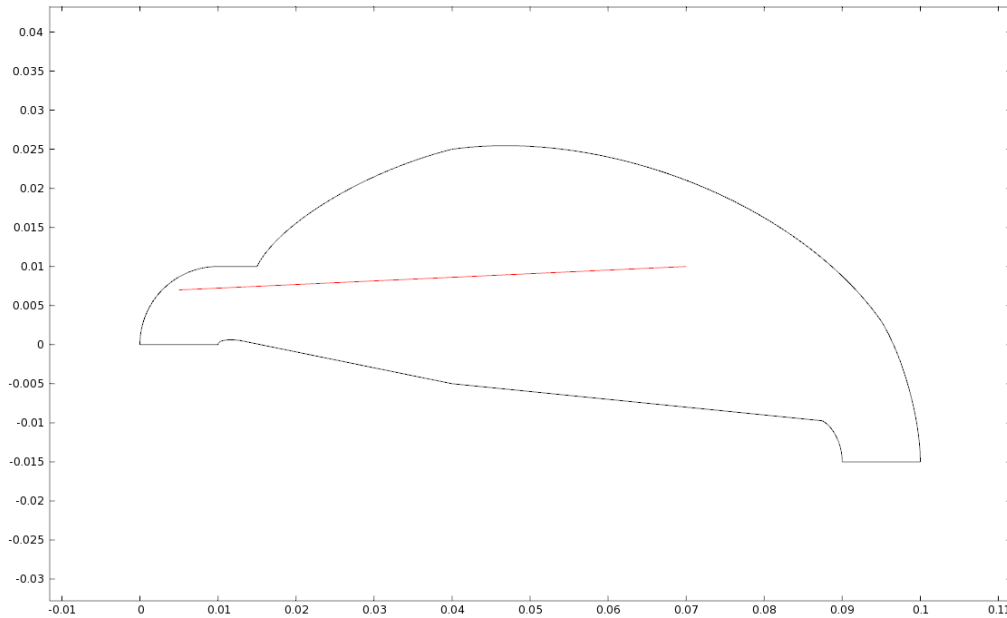


Figure 12. Schematic of a nasal cavity. The red line located in the middle of the cavity is where the average velocity is taken for the mesh convergence analysis

The mesh convergence analysis was performed based on the average value of the velocity along the red line shown in Figure 12 because the velocity field varies the most in this region. The average velocity was evaluated at eight different mesh sizes, and the solution began to converge when number of elements reached 5563 (Figure 13). This mesh was used as our model to evaluate the drug deposition for our final solution.

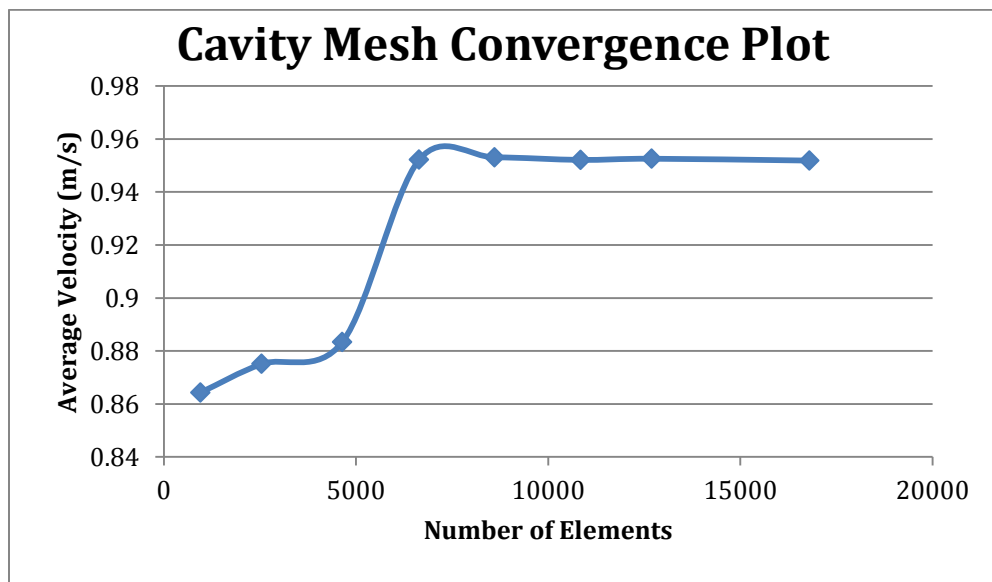


Figure 13. Mesh convergence analysis of nasal cavity.

Mesh convergence was also performed on the mucosal layer subdomain (Figure 14). Analysis was performed at 5 different mesh sizes by integrating drug concentration across the mucosal domain after 1 hour. The solution converges at about 5000 elements and our mesh contained 5678 elements. This mesh was used in our mass transport model.

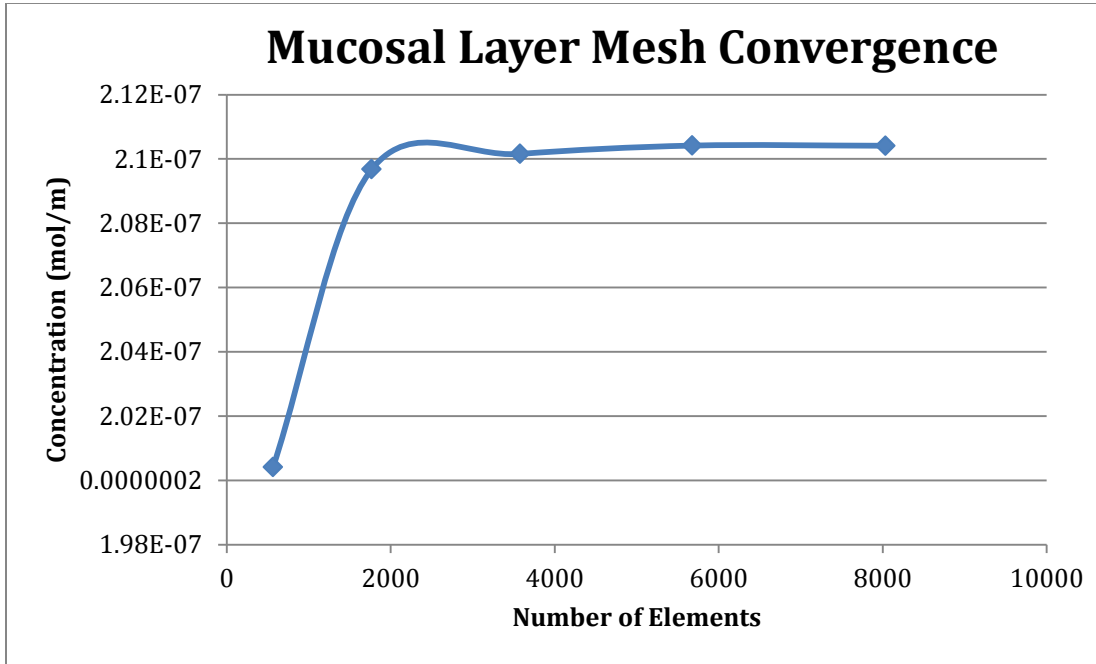


Figure 14. Mesh convergence analysis of mucosal layer.

8. Appendix C: Software Implementation

8.1 Particle Tracing

To obtain particle trajectory plot, we used a COMSOL particle tracing feature under post-processing. This function requires five major input parameters including force equation derived in section 6.1, particle mass, particle initial positions, and initial velocity of the particles. These respective parameters indicated by number 1-5 were input into the particle tracing window shown in Figure 15.

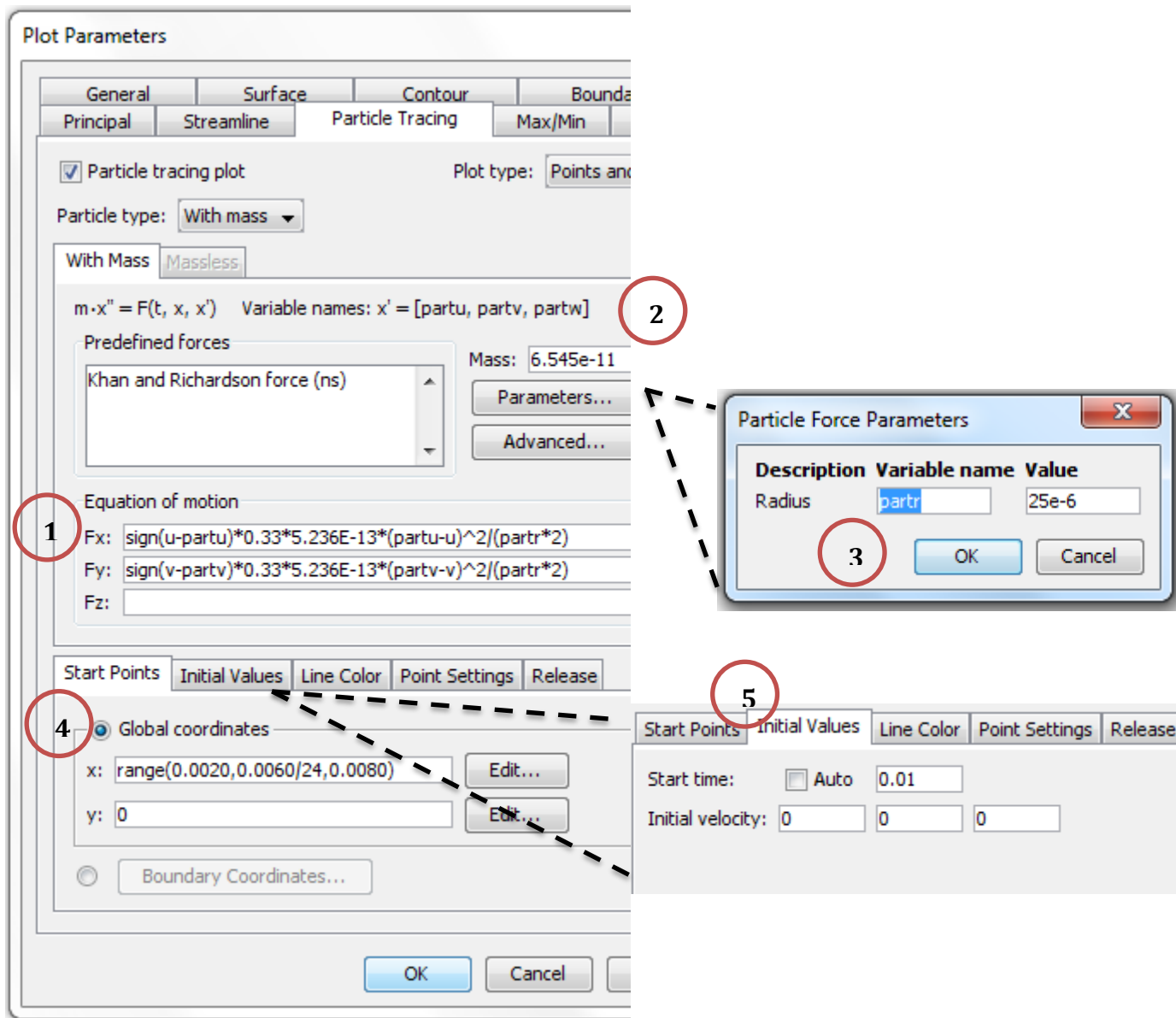


Figure 15. COMSOL particle tracing window. Number 1-5 indicate the five required input parameters: force, particle mass, particle radius, particle release positions, and initial velocity, respectively

8.2 Particle Coordinates

To determine particle position along the boundary, we exported our model in FEM format into MATLAB. The following code was used to run the particle simulation in MATLAB for 25 particles and extract particle position (Figure 16).

```
x = linspace(0.002,0.008,25);
y = linspace(0,0,25);

A = [x; y];

h = postplot(fem,...
    'partstart',A,...
    'parttstart', 0.01,...
    'partmass','6.545e-11',...
    'parttvar','partt',...
    'partdata',{'u','v'},...
    'partedgetol',0.0001,...
    'partforce',['sign(u-partu)*0.33*5.236E-13*(partu-u)^2/(25e-6*2)';
'sign(y-party)*0.33*5.236E-13*(party-y)^2/(25e-6*2)'],...
    'partstatic',{'off'},...
    'partrtol',0.0001,...
    'parthmax','auto',...
    'outtype','postdata');

m = cell2mat(h);
```

Figure 16. MATLAB code for FEM simulation of particle module

9. Appendix D: References

Bateman, N.D, A.D Whymark, N.J Clifton, and T.J Woolford. "A Study of Intranasal Distribution of Azelastine Hydrochloride Aqueous Nasal Spray with Different Spray Techniques." *Clinical Otolaryngology*. 27.5 (2002): 327-330. Print.

Berger, W.E. "Pharmacokinetic Characteristics and Safety and Tolerability of a Reformulated Azelastine Hydrochloride Nasal Spray in Patients with Chronic Rhinitis." *Expert Opinion on Drug Metabolism and Toxicology*. 5.1 (2009): 91-102. Print.

Braver, H. M., A. J. Block, and M. G. Perri. "Treatment for Snoring: Combined Weight Loss, Sleeping on Side, and Nasal Spray." *Chest* 107.5 (1995): 1283-288. Print.

Cheng, YS, TD Holmes, J Gao, RA Guilmette, S Li, Y Surakitbanharn, and C Rowlings. "Characterization of Nasal Spray Pumps and Deposition Pattern in a Replica of the Human Nasal Airway." *Journal of Aerosol Medicine : the Official Journal of the International Society for Aerosols in Medicine*. 14.2 (2001): 267-80. Print.

"Compound Report Card." *ChEMBL*. EMBL-EBI. Web. 30 Apr. 2012. <<https://www.ebi.ac.uk/chembl/index.php/compound/inspect/CHEMBL639>>.

Dashe, Alfred M., Charles B. Kleeman, J. Walter Czaczkes, Howard Rubinoff, and Irene Spears. "Synthetic Vasopressin Nasal Spray in the Treatment of Diabetes Insipidus." *Synthetic Vasopressin Nasal Spray in the Treatment of Diabetes Insipidus*. Web. 27 Apr. 2012. <<http://jama.ama-assn.org/content/190/12/1069.short>>.

Datta, Ashim K., and Vineet Rakesh. *An Introduction to Modeling of Transport Processes: Applications to Biomedical Systems*. Cambridge, UK: Cambridge UP, 2010. Print.

Desai, M. A., & Vadgama, P. (January 01, 1991). Estimation of effective diffusion coefficients of model solutes through gastric mucus: assessment of a diffusion chamber technique based on spectrophotometric analysis. *The Analyst*, 116, 11, 1113-6.

Efficient Drug Delivery Using Computational Fluid Dynamics." *Computers in Biology and Medicine* 38.6 (2008): 713-26. Print.

Hansen, M. S., O. Mathiesen, S. Trautner, and J. B. Dahl. "Intranasal Fentanyl in the Treatment of Acute Pain - a Systematic Review." *Acta Anaesthesiol Scand* 56 (2012): 407-19. Print.

Holland FA and R Bragg, 1995. Fluid Flow for Chemical Engineers (2nd Edition). Elsevier. Online version available at: http://knovel.com/web/portal/browse/display?_EXT_KNOVEL_DISPLAY_b

okid=412&VerticalID=0

Hua, X., Zeman, K. L., Zhou, B., Hua, Q., Senior, B. A., Tilley, S. L., & Bennett, W. D. (January 01, 2010). Noninvasive real-time measurement of nasal mucociliary clearance in mice by pinhole gamma scintigraphy. *Journal of Applied Physiology*, 17, 1, 189.

Inthavong, K., Z F. Tian, H F. Li, J Y. Tu, W Yang, C L. Xue, and C G. Li. "A Numerical Study of Spray Particle Deposition in a Human Nasal Cavity." *Aerosol Science & Technology*. 40.11 (2006): 1034-1045. Print.

Inthavong, K., Z. Tian, J. Tu, W. Yang, and C. Xue. "Optimising Nasal Spray Parameters for Efficient Drug Delivery Using Computational Fluid Dynamics." *Computers in Biology and Medicine* 38.6 (2008): 713-26. Print.

Martin, E., Schipper, N. G., Verhoef, J. C., & Merkus, F. W. (January 01, 1998). Nasal mucociliary clearance as a factor in nasal drug delivery. *Advanced Drug Delivery Reviews*, 29, 13-38.

Quraishi, MS, NS Jones, and JD Mason. "The Nasal Delivery of Drugs." *Clinical Otolaryngology and Allied Sciences*. 22.4 (1997): 289-301. Print.

Schoenwetter, W. F., Dupclay, L., Appajosyula, S., Botteman, M. F., & Pashos, C. L. (January 01, 2004). Economic impact and quality-of-life burden of allergic rhinitis. *Current Medical Research & Opinion*, 20, 3, 305-317.

Zia, H, P Dondeti, and T E. Needham. "Intranasal Drug Delivery." *Clinical Research and Regulatory Affairs*. 10.2 (1993): 99-135. Print.